CHEMISTRY
A EUROPEAN JOURNAL

DOI: 10.1002/chem.200500802

Computational Study of Solvent Effects and the Vibrational Spectra of Anderson Polyoxometalates

Adam J. Bridgeman*[a]

Abstract: The structures and vibrational frequencies of the type II Anderson heteropolyanions $[TeMo_6O_{24}]^{6-}$ and $[IMo_6O_{24}]^{5-}$have been calculated by using density functional theory using a number of common functionals and basis sets. For the first time, Raman intensities have been calculated and the effect of solvent on the modeling has been investigated. The calculated IR and Raman spectral traces are in good agreement with experiment allowing the characteristic group frequencies for this class of polyoxometalate to be identified. The stretching vibrations of the molybdenum–oxygen bonds are predicted to occur at somewhat lower frequencies than in the type I polyoxometalates. Stretching of the heteroatom–oxygen bonds occurs at significantly lower frequencies than in the Keggin anions as a simple consequence of the higher coordination number of the central heteroatom in the Anderson systems. For the $[Mo_2O_7]^{2-}$ and $[Mo_6O_{19}]^{2-}$ ions, the relatively low negative charge leads to small structural changes when solvent is included. In these systems, solvent leads to an increase in the bond polarity and a decrease in the covalent bond orders, resulting in decreases in the calculated frequencies. For the Anderson anions, the higher negative charges leads to greater solvent effects with contraction of the clusters and increases in the frequencies of bands due to stretching of the two, *cis*-related molybdenum–oxygen bonds.

Keywords: Anderson anions · density functional calculations · polyoxometalates · solvent effects · vibrational spectroscopy

Introduction

Polyoxometalates (POMs) constitute an extremely diverse class of medium-to-large inorganic metal–oxygen cluster compounds.[1,2] They have quite remarkable chemical and physical properties with applications in a wide variety of areas, including medicine, catalysis, solid-state technology and chemical analysis.[3,4] They are primarily built by edge and, occasionally, corner sharing of MO_n polyhedra, where n is most commonly equal to six. The resulting cages are usually approximately spherical. Heteropolyoxometalates have a general chemical formula $[X_nM_pO_q]^{z-}$, where M is most commonly Mo or W and X is a main-group or transition-metal heteroatom. The vast majority of POMs contain no more than two unshared, or 'terminal', in each MO_n polyhedron. In the Pope classification,[1,2] type-I POMs contain only one metal–oxo terminal group and type-II systems contain two, *cis*-related metal–oxo groups in each polyhedron, as shown in Scheme 1a and b, respectively.

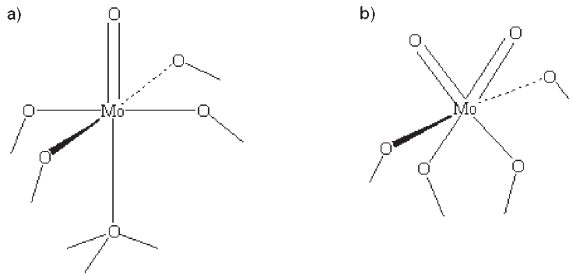

Scheme 1.

The most important heteropolyoxometalates are undoubtably the Keggin anions which have the formula $[XM_{12}O_{40}]^{z-}$ The α-Keggin structure consists of an assemblage of (distorted) $[MO_6]$ octahedra and a $[XO_4]$ tetrahedron. The ion exhibits ideal T_d symmetry and all M atoms are equivalent, occupying the centres of distorted C_s octahedra with one terminal $M{-}O_t$ bond. They are thus representative of the type-I class of POMs. Anderson heteropolyoxometalates have the general formula $[XM_6O_{24}]^{z-}$. The Anderson structure,

[a] Dr. A. J. Bridgeman
Department of Chemistry, University of Hull
Kingston-upon-Hull, HU6 7RX (UK)
Fax: (+44) 1482-466-410
E-mail: a.j.bridgeman@hull.ac.uk

shown in polyhedral representation in Figure 1a, consists of a "ring" of six, distorted MO_6 octahedra and a central, distorted XO_6 octahedron. Figure 1b shows the structure in a ball-and-stick representation, which reveals the extent of the distortion of the MO_6 octahedra. As shown in Figure 1 b, the MO_6 units are edge-shared through M-O-M bridges provided by two coordinate (O_{2c}, O2) and three coordinate (O_{3c}, O3) oxygen atoms. The latter are connected to both the M and X atoms. Each MO_6 unit has two, *cis*-related M–O terminal groups. The Anderson structure is thus representative

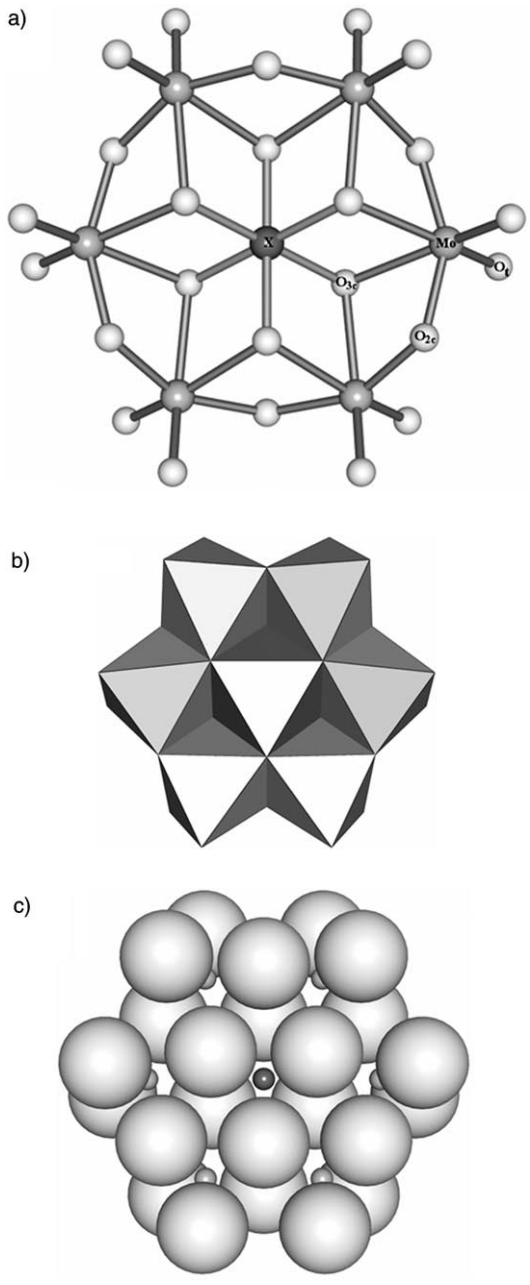

Figure 1. Structure and atom labelling for an Anderson anion showing a) individual atoms and bonds, b) the assemblage of six $[MO_6]$ octahedra around the central $[XO_6]$ octahedron and c) two pseudo-closed packed layers of oxygen atoms with the metal and heteroatom in distorted octahedral holes.

of the type-II class of POMs. Figure 1c shows the structure as two pseudo-closed packed layers of twelve oxygen atoms with the metal and heteroatom in the octahedral holes between the layers.

Vibrational spectroscopy is an important tool in probing of the structures and dynamics of POMs.[5] However, the assignment of the vibrational spectra of these clusters anions is problematic and complicated due to both their large size and structural complexity. We have recently completed detailed computational studies of the vibrational frequencies and assignments of the type-I Lindqvist[6] and α- and β-Keggin[7,8] anions. The study of the Lindqvist anions was the first high-level computational modelling of the vibrational spectra of POMs to be published. It contained an examination of the accuracy of various computational methods. Vibrational analyses on large anions such as these are extremely computationally demanding, requiring accurate geometries and treatment of electron correlation and relativistic effects. The Hartree–Fock method, for example, is able to reproduce the geometries of these anions quite well but performs very poorly when applied to vibrational frequencies. As well as providing exacting tests of the available computational methods, these studies allowed the vibrational spectra to be assigned leading, in a number of cases, to reassignment and clarification of earlier work.

Herein a computational study of the vibrational spectra of the Anderson heteropolyoxometalates $[TeMo_6O_{24}]^{6-}$ and $[IMo_6O_{24}]^{5-}$ is reported As type-II systems, these POMs represent an extremely useful set to use as a comparison with the type-I anions previously investigated. Their high symmetry also reduces, somewhat, the computational requirements. However, our previous work on reduced Lindqvist anions[6] highlighted relatively poor performance of the computational methods on POMs with highly negative charges. Type-II POMs necessarily tend to have such charges. The study reported here thus extends our previous work by investigating solvent effects on the computational modelling. Studies of the effect of solvent on the calculated properties of POMs are still in their infancy[9,10] and have been restricted thus far to energetic and structural issues. The study reported here represents the first high-level investigation of the effect of solvent in the modelling of the vibrational spectra of POMs.

Computational Approach

In our previous study of the vibrational spectra of Lindqvist isopolyanions,[6] we examined the performance of a variety of computational methods. The results suggested that the local density approximation (LDA) with triple-ζ Slater-type orbitals (STO) and the zero-order regular approximation (ZORA) relativistic approach implemented within the ADF program[11,12] is best able to model both the structure and vibrational spectra of these polyanions when treated as pseudo-gas phase species. However, the ADF program uses numerical differentiation of analytic first derivatives of the energy to calculate vibrational frequencies. This approach

requires a large number of single point calculations at geometries close to the equilibrium structure, requiring high self-consistent field (SCF) convergence and integration accuracy for large clusters with no symmetry. In our comparative study of the vibrational spectra of α and β-Keggin anions,[7,8] this approach proved *extremely* computationally demanding but considerably more reliable than methods based on Gaussian-type orbitals. For the $[TeMo_6O_{24}]^{6-}$ and $[IMo_6O_{24}]^{5-}$ ions, calculations are reported with triple-ζ STO (ADF type TZP) basis orbitals for all atoms incorporating frozen cores (ADF type Mo.3d, O.1 s, Te.4p and I.4p) and the ZORA relativistic approach[11] and the Vosko–Wilk–Nusair (VWN) form of the local density approximation.[13]

Our study of the Lindqvist anions included modelling of the clusters with high negative charges. For these systems, even the LDA approach performed relatively poorly. Lopez et al. have recently published a detailed study[10] of the effects of solvent on the modelling of the structures and energetics of POMs. Given the relatively high negative charge on the Anderson anions of interest in this paper, inclusion of environmental effects is also likely to be important in modelling their vibrational behaviour. In this paper, we report, to the best of our knowledge, the first high-level study on the effect of solvent on the calculated vibrational frequencies of POMs. The effect of the dielectric constant of the solvent on the vibrational frequencies of the simple dimolybdate $[Mo_2O_7]^{2-}$ ion is reported, using the computational method outlined above. For the Anderson anions, we report a comparison of LDA and BP86[14] calculations using the ADF triple-ζ basis sets including polarization functions (TZP), denoted as "LDA/TZP" and "BP86/TZP" respectively, in and out of solvent and B3LYP calculations.[15] The latter have been performed using the analytical second derivatives available in the Gaussian 98[16] program with LANL2DZ basis sets which feature quasi-relativistic effective core potentials to represent the atomic cores and double-ζ quality GTO for the valence orbitals. For the central main-group element, the LANL2DZ basis set has been augmented with additional polarization functions, denoted as LANL2DZ(P). Unfortunately, use of the B3LYP/LANL2DZ(P) model in solvent led to severe SCF convergence problems so that a comparison of its performance is restricted to gas-phase modelling only. The conductor-like screening model COSMO[17] was used for solvation (water $\varepsilon = 78$).

For $[TeMo_6O_{24}]^{6-}$, Raman scattering intensities have also been calculated by using the ADF program. Analogous to the calculation of the IR spectrum, this computes the dipole polarizability tensor for geometries close to the equilibrium structure leading to long computational times. Very few calculations of this type have been reported on molecules of this size and, to the best of our knowledge, the calculations reported here are the first on Raman intensities for POMs.

Spectral traces have been plotted using "spectralPlot"[18] assuming Lorentzian band shapes and with an average band width chosen to reflect that found experimentally. Bond orders were calculated by using the definition proposed by Mayer[19] respectively using the MAYER program.[20]

Results and Discussion

Structures of the $[TeMo_6O_{24}]^{6-}$ and $[IMo_6O_{24}]^{5-}$ anions: We have previously reported[21] a detailed comparison of the electronic structure of type-I and -II heteropolyoxometalates at the LDA/TZIP level, including $[TeMo_6O_{24}]^{6-}$. Table 1 lists optimized M–O and X–O bond lengths for $[TeMo_6O_{24}]^{6-}$ from that study and using the additional methods used here and for $[IMo_6O_{24}]^{5-}$ together with the available experimentally determined distances[22,23] at each of the computational levels used for the vibrational modelling. The vibrational analyses reported below confirm that these ions have full D_{3d} symmetry respectively in the gas phase, as assumed in our earlier computational studies of the structures of these anions[21] as well as in solution.

The agreement between the crystallographic and calculated bond lengths is reasonable at all levels. In keeping with previous computational studies of POMs,[24–26] bond lengths are over estimated particularly for terminal and heteroatom–oxygen bonds. The $Mo–O_{2c}$ bond lengths are well reproduced at all levels. As we have noted previously,[6,25] the LDA approach appears best able to reproduce solid state bond lengths. This presumably reflects a compensation for the lack of the stabilizing crystal field in pseudo-gas phase calculations by the overbinding associated with the local density method. Inclusion of solvent leads to a shortening of the $Mo–O_t$, $Mo–O_{2c}$ and X–O bonds with similar effects at the LDA and BP86 levels. Inclusion of the stabilization of the anion by the solvent leads to bond lengths which approach those observed in the solid so that solvation appears, at least to a first approximation, to act in similar way to the crystal-field effect experienced by the anion in the solid state.

Table 1. Calculated bond lengths [Å] for $[TeMo_6O_{24}]^{6-}$ and $[IMo_6O_{24}]^{5-}$ together with experimentally determined values. The atom labelling corresponds to that used in Figure 1.

	$[TeMo_6O_{24}]^{6-}$					$[IMo_6O_{24}]^{5-}$				
	Te–O	$Mo–O_t$	$Mo–O_{2c}$	$Mo–O_{3c}$	Ref.	I–O	$Mo–O_t$	$Mo–O_{2c}$	$Mo–O_{3c}$	Ref.
LDA/TZP	1.99	1.76	1.94	2.27	[21]	1.95	1.74	1.93	2.32	
LDA/TZIP/Sol	1.98	1.74	1.93	2.26		1.94	1.72	1.93	2.30	
BP86/TZP	2.02	1.77	1.96	2.33		1.98	1.76	1.95	2.39	
BP86/TZP/Sol	2.00	1.76	1.96	2.31		1.96	1.75	1.95	2.37	
B3LYP/LANL2DZ(P)	2.00	1.77	1.96	2.35		1.96	1.76	1.95	2.43	
crystallographic	1.93	1.72	1.94	2.28	[22]	1.89	1.71	1.92	2.34	[23]

Assignment of the vibrational spectra of the $[TeMo_6O_{24}]^{6-}$ and $[IMo_6O_{24}]^{5-}$ ions: The thirty-one atom Anderson POMs have 87 normal modes. For the D_{3d} structures, these span:

$$\Gamma_{vib} = 8a_{1g}\ (\text{Raman}) + 14e_g\ (\text{Raman}) + 9a_{2u}\ (\text{IR}) + 15e_u\ (\text{IR}) + 6a_{2g} + 6a_{1u} \quad (1)$$

where the IR and Raman activities are shown in parenthesis. Twenty-four IR bands and twenty-two non-coincident Raman bands might therefore, in principle, be expected. Table 2 and Table 3 list the calculated frequencies and assignments for the $[TeMo_6O_{24}]^{6-}$ and $[IMo_6O_{24}]^{5-}$ ions at the LDA/TZIP levels, together with available experimental frequencies.[27,28] Figure 2 shows the calculated and observed IR and Raman spectral traces for $[TeMo_6O_{24}]^{6-}$. An interactive model of the IR and Raman spectra of $[TeMo_6O_{24}]^{6-}$, showing animations of the normal modes, is available on our website.[29] The descriptions of the vibrations in Table 2 and Table 3 and below are necessarily approximate as many modes correspond to complex motions of the whole cluster. The website is provided to show the modes in more detail. Overall, the calculated frequencies appear to be in reasonable agreement with those observed experimentally. As might be anticipated by our previous studies of highly charged anions[6] and by the over-estimation of the bond lengths noted above, the calculated frequencies are uniformly at lower frequency than the experimental values. In support of this observation, it should be noted that the frequencies of the iodomolybdate are calculated to be higher than those of the telluromolybdate. This is presumably simply due to its lower negative charge as its bond lengths and bond orders are very similar. Reproduction of spectral traces is a more exacting test of the model. Whilst the Raman spectrum is reasonably well reproduced, the calculated IR spectrum below $700\ cm^{-1}$ is in poor agreement with the experimental trace. This is, in part, due to the low calculated intensity in this region and, in part, due to the complication of bands due to the counter ions in the experimental trace.

Previous workers have followed the assignment of the bands given by Grabowski et al.[27] and by Dengel et al.,[28] based on restricted force constant analysis and on comparison with related systems. The highest energy vibrations, above $900\ cm^{-1}$, can be readily assigned to the symmetric and asymmetric stretches of the *cis*-$Mo(O_t)_2$ unit. Experimentally, bands are observed in the IR and Raman spectra in this region which can be readily assigned on the basis of their position and intensity. For the *cis*-$Mo(O_t)_2$ units, the twelve stretching modes span $a_{1g} + a_{2g} + 2e_g + a_{1u} + a_{2u} + 2e_u$, giving rise to, potentially, three IR and three Raman bands.

Table 2. Calculated (LDA/TZP) and experimental[27] vibrational frequencies (in cm^{-1}) and approximate descriptions for $[TeMo_6O_{24}]^{6-}$. The calculated IR [km mol^{-1}] and Raman (R) intensities [$Å^4$ amu^{-1}] are given in parenthesis. The vibrations below $350\ cm^{-1}$ involve motions of the whole cage.

Mode		Calcd	Obsd	Assignment
a_{1g}	ν_1	900 (350: R)	950 (s)	ν_s ($Mo(O_t)_2$)
e_u	ν_{44}	882 (1390: IR)	950 (s)	ν_s ($Mo(O_t)_2$)
a_{2u}	ν_{35}	876 (1130: IR)	930 (s)	ν_{as} ($Mo(O_t)_2$)
e_g	ν_{15}	872 (82: R)	900 (s)	ν_s ($Mo(O_t)_2$)
a_{1u}	ν_{29}	868		ν_s (Mo–O_t), ν_s (Mo-O_{2c}-Mo)
e_g	ν_{16}	862 (164: R)	885 (s)	ν_{as} (Mo–O_t), ν_{as} (Te-O_{3c})
e_u	ν_{45}	847 (396: IR)	908 (s)	ν_{as} ($Mo(O_t)_2$)
a_{2g}	ν_9	836		ν_{as} ($Mo(O_t)_2$)
a_{1u}	ν_{30}	741		ν_s (Mo-O_{2c}-Mo)
e_g	ν_{17}	730 (8: R)		ν_s (Mo-O_{2c}-Mo)
e_u	ν_{46}	679 (4100: IR)	690 (s)	ν_{as} (Mo-O_{2c}-Mo)
a_{1g}	ν_2	615 (7: R)	685 (s)	ν_s (Te–O_{3c})
e_u	ν_{47}	581 (12: IR)	620 (s)	ν_{as} (Te–O_{3c})
a_{2u}	ν_{36}	579 (34: IR)	545 (sh)	ν_{as} (Te–O_{3c})
e_g	ν_{18}	565 (8: R)	560	ν_s (Te–O_{3c})
a_{1g}	ν_3	535 (8: R)		ν_s (Te–O_{3c}), δ (Mo-O_{2c}-Mo)
e_u	ν_{48}	532 (36: IR)		δ (Mo-O_{2c}-Mo)
a_{2g}	ν_{10}	530		ν_{as} (Mo-O_{2c}-Mo)
e_g	ν_{19}	528 (6: R)		ν_s (Te–O_{3c}), δ (Mo-O_{3c}-Mo)
a_{2u}	ν_{37}	521 (0.2: IR)		ν_s (Te–O_{3c}), δ (Mo-O_{3c}-Mo)
a_{2u}	ν_{38}	459 (76: IR)	500 (sh)	δ (O_{3c}-Te-O_{3c}), δ (Mo-O_{3c}-Mo)
e_g	ν_{20}	445 (3: R)		δ (O_{3c}-Te-O_{3c})
e_u	ν_{49}	431 (311: IR)	465 (sh)	δ (O_{3c}-Te-O_{3c})
a_{1g}	ν_4	396 (0.5: R)		δ (Mo-O_{2c}-Mo), δ (Mo-O_{3c}-Mo)
a_{1u}	ν_{31}	392		δ (O_{3c}-Te-O_{3c})
a_{1g}	ν_5	355 (6: R)		δ (Mo-O_{2c}-Mo), δ (Mo-O_{3c}-Mo)
e_u	ν_{50}	354 (190: IR)		δ (Mo-O_{2c}-Mo), δ (Mo-O_{3c}-Mo)

Mode		Calcd	Mode		Calcd
e_g	ν_{21}	339 (14: R)	a_{2u}	ν_{41}	186 (4: IR)
a_{1u}	ν_{32}	331	e_g	ν_{25}	181 (16: R)
e_u	ν_{51}	321 (19: IR)	e_g	ν_{26}	177 (2: R)
e_g	ν_{22}	317 (14: R)	e_u	ν_{55}	176 (2: IR)
a_{2u}	ν_{39}	302 (9: IR)	a_{1g}	ν_8	128 (14: R)
e_u	ν_{52}	301 (2: IR)	e_u	ν_{56}	115 (4: IR)
a_{1g}	ν_6	299 (6: R)	e_u	ν_{57}	97 (0.4: IR)
e_g	ν_{23}	298 (3: R)	e_g	ν_{27}	93 (3: R)
a_{2g}	ν_{11}	275	a_{2u}	ν_{42}	91 (1: IR)
a_{2u}	ν_{40}	233 (3: IR)	a_{2g}	ν_{13}	90
e_u	ν_{53}	230 (4: IR)	a_{1u}	ν_{34}	90
e_u	ν_{54}	213 (46: IR)	e_g	ν_{28}	78 (6: R)
e_g	ν_{24}	210 (19: R)	a_{2u}	ν_{43}	69 (0: IR)
a_{1g}	ν_7	204 (25: R)	e_u	ν_{58}	35 (1: IR)
a_{1u}	ν_{33}	200	a_{2g}	ν_{14}	35
a_{2g}	ν_{12}	196			

Table 3. Calculated (LDA/TZP) and experimental[28] vibrational frequencies (in cm^{-1}) and approximate descriptions for $[IMo_6O_{24}]^{5-}$. IR intensities ($km\,mol^{-1}$) are given in parenthesis. The vibrations below 350 cm^{-1} involve motions of the whole cage.

Mode		Calcd	Obsd	Assignment
a_{1g}	ν_1	926	961	ν_s ($Mo(O_t)_2$)
e_u	ν_{44}	925 (1200)	946 (br)	ν_s ($Mo(O_t)_2$)
e_g	ν_{15}	909	938	ν_s ($Mo(O_t)_2$)
a_{1u}	ν_{29}	900		ν_s (Mo–O_t), ν_s (Mo-O_{2c}-Mo)
a_{2g}	ν_9	896		ν_{as} ($Mo(O_t)_2$)
e_g	ν_{16}	894	925	ν_{as} (Mo–O_t), ν_{as} (I–O_{3c})
a_{2u}	ν_{35}	888 (1021)	911 (s)	ν_{as} ($Mo(O_t)_2$)
e_u	ν_{45}	878 (354)		ν_{as} ($Mo(O_t)_2$)
a_{1u}	ν_{30}	767		ν_s (Mo-O_{2c}-Mo)
e_g	ν_{17}	756	719	ν_s (Mo-O_{2c}-Mo)
e_u	ν_{46}	703 (2047)	722 (br)	ν_{as} (Mo-O_{2c}-Mo)
a_{1g}	ν_2	619	680	ν_s (I–O_{3c})
e_u	ν_{47}	595 (0.4)	634	ν_{as} (I–O_{3c})
a_{2u}	ν_{36}	587 (42)	598 (s)	ν_{as} (I–O_{3c})
e_g	ν_{18}	574		ν_s (I–O_{3c})
a_{2g}	ν_{10}	548		ν_{as} (Mo-O_{2c}-Mo)
a_{2u}	ν_{37}	548 (3)		ν_s (I–O_{3c}), δ (Mo-O_{3c}-Mo)
e_g	ν_{19}	540		ν_s (I–O_{3c}), δ (Mo-O_{3c}-Mo)
a_{1g}	ν_3	526		ν_{as} (I–O_{3c}), δ (Mo-O_{2c}-Mo)
e_u	ν_{48}	526 (42)		δ (Mo-O_{2c}-Mo)
a_{2u}	ν_{38}	454 (57)		ν_s (I-O_{3c}), δ (Mo-O_{3c}-Mo)
e_g	ν_{20}	448		δ (O_{3c}-I-O_{3c}), δ (Mo-O_{3c}-Mo)
e_u	ν_{49}	443 (440)	473 (m)	δ (O_{3c}-I-O_{3c})
a_{1g}	ν_4	397	389	δ (Mo-O_{2c}-Mo), δ (Mo-O_{3c}-Mo)
a_{1u}	ν_{31}	381		δ (O_{3c}-I-O_{3c})
a_{1g}	ν_5	362		δ (Mo-O_{2c}-Mo), δ (Mo-O_{3c}-Mo)
e_u	ν_{50}	351 (260)		δ (Mo-O_{2c}-Mo), δ (Mo-O_{3c}-Mo)
a_{1u}	ν_{32}	350		δ (Mo-O_{2c}-Mo), δ (Mo-O_{3c}-Mo)

Mode		Calcd	Mode		Calcd
e_g	ν_{21}	349	e_u	ν_{54}	203 (5)
e_u	ν_{51}	323 (42)	e_g	ν_{25}	188
a_{2u}	ν_{39}	319 (12)	e_u	ν_{55}	182 (2)
e_g	ν_{22}	314	e_g	ν_{26}	176
e_u	ν_{52}	303 (10)	e_u	ν_{56}	129 (2)
a_{1g}	ν_6	301	a_{1g}	ν_8	118
e_g	ν_{23}	293	a_{2u}	ν_{42}	103 (0.5)
a_{2g}	ν_{11}	256	a_{2g}	ν_{13}	98
a_{2u}	ν_{40}	232 (1)	e_g	ν_{27}	96
e_u	ν_{53}	229 (28)	a_{1u}	ν_{34}	92
a_{1u}	ν_{33}	225	e_g	ν_{57}	91 (2)
e_g	ν_{24}	215	e_g	ν_{28}	81
a_{2g}	ν_{12}	205	a_{2u}	ν_{43}	68 (0.1)
a_{1g}	ν_7	204	a_{2g}	ν_{14}	37
a_{1u}	ν_{33}	204	e_u	ν_{58}	20
a_{2u}	ν_{41}	204 (4)			

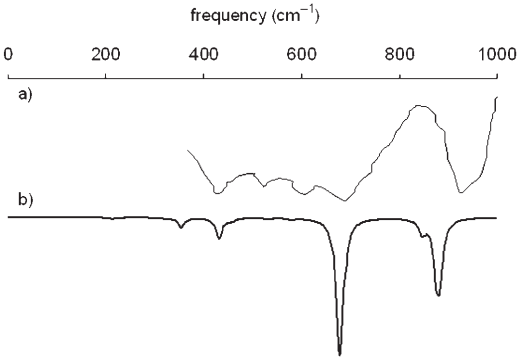

Figure 2. a) Calculated and b) observed IR traces for $[TeMo_6O_{24}]^{6-}$. The observed trace is adapted from that in reference [27].

For $[TeMo_6O_{24}]^{6-}$, the IR shows strong absorptions at 950, 930 and 908 cm^{-1} and they can be assigned to e_u (ν_{44}), a_{2u} (ν_{35}) and e_u (ν_{45}) respectively. The latter corresponds to asymmetric motion of the two Mo–O_t bonds and the former to their symmetric stretch. The IR activity of the latter arises due to the coupling between the type-II centres. The Raman spectrum (Figure 3) shows bands at 950 and 900 cm^{-1} and these may be assigned to the a_{1g} (ν_1) and e_g (ν_{15}) modes which both correspond to symmetric stretches of the two Mo–O_t bonds.

For $[IMo_6O_{24}]^{5-}$, the IR shows strong bands at 946 cm^{-1} and 911 cm^{-1} and these may be readily assigned, as in the telluromolybdate, to the e_u (ν_{44}) and a_{2u} (ν_{35}) modes respectively. The e_u (ν_{45}) has a very similar calculated frequency to the latter and presumably occurs under the much more intense a_{2u} (ν_{35}) absorption. Dengel et al.[28] assigned the 946 cm^{-1} to an asymmetric stretch of the $Mo(O_t)_2$ bonds. The e_u (ν_{44}) mode involves a symmetric stretch and the IR intensity is derived from the coupling between the type-II centres. The Raman spectrum shows intense peaks at 961 and 938 cm^{-1} and these may be assigned to the a_{1g} (ν_1), e_g (ν_{15}) stretches.

Absorptions between 690 and 730 cm^{-1} are due to stretches of the Mo-O_{2c}-Mo bonds. In the telluromolybdate, the IR peak at 690 cm^{-1} is assigned to the e_u (ν_{46}) asymmetric stretch of the two *trans*-related Mo–O_{2c} bonds on each metal centre. In the iodo system, the IR peak at 722 cm^{-1} can be assigned to the e_u (ν_{46}) mode whilst the Raman peak at 719 cm^{-1} can be assigned to the corresponding e_g (ν_{17}) symmetric stretch . Dengel et al. assigned these peaks to vibrations of the central $[XO_6]$ unit. These are calculated to occur at between 570 and 620 cm^{-1}. The six stretching modes of the trigonally distorted $[XO_6]$ octahedron span $a_{1g} + e_g + a_{2u} + e_u$, giving rise, potentially, to two IR and two Raman bands. For $[TeMo_6O_{24}]^{6-}$, the IR bands at 620 and 545 cm^{-1} are assigned to the e_u (ν_{48}) and

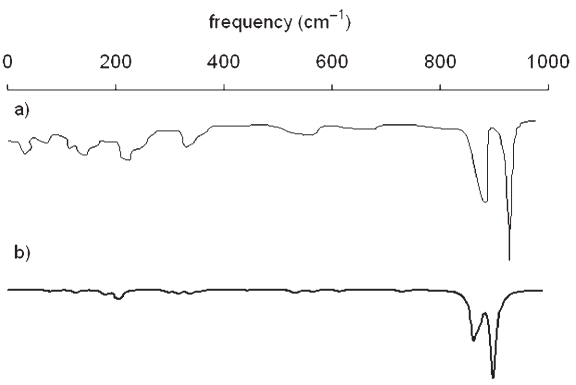

Figure 3. a) Calculated and b) observed Raman traces for $[TeMo_6O_{24}]^{6-}$. The observed trace is adapted from that in reference [28].

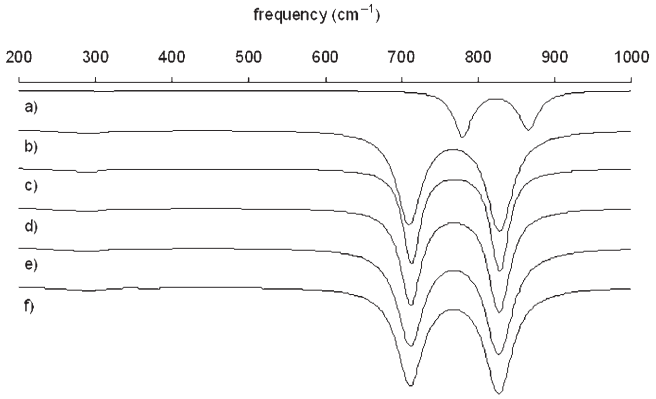

Figure 4. Calculated IR trace for $[Mo_2O_7]^{2-}$ in the presence of solvent with varying dielectric constant, $\varepsilon = 0$ (a), 20 (b), 40 (c), 60 (d), 80 (e) and 100 (f).

a_{2u} (ν_{36}) asymmetric stretches of the $[TeO_6]$ unit. The Raman peak at 680 cm^{-1} is assigned to the a_{1g} (ν_2) "breathing mode". The Raman peak at 560 cm^{-1} could be due to either the e_g (ν_{18}) or a_{1g} (ν_3) modes, or to an overlapping combination. For $[IMo_6O_{24}]^{5-}$, the IR bands at 634 and 598 cm^{-1} and the Raman peak at 680 cm^{-1} can be similarly assigned to the e_u (ν_{48}), a_{2u} (ν_{36}) and a_{1g} (ν_2) modes, respectively.

Below these frequencies, assignments to individual functional groups become less clear as the vibrations involve bending motions which, necessarily in a cluster, tend to involve movement of many atoms. The peaks at 500 and 465 cm^{-1} in the IR spectrum of $[TeMo_6O_{24}]^{6-}$, can be assigned to the a_{2u} (ν_{38}) and e_u (ν_{49}) modes, respectively, which involve bending of the O-Te-O bonds. For the iodo system, the IR peak at 473 cm^{-1} is assigned to the e_u (ν_{49}) mode whilst the Raman peak at 389 cm^{-1} is assigned to either the a_{1g} (ν_4) or a_{1g} (ν_5) mode mode, both of which are predicted to occur in this region and both of which involve bending of the Mo_6O_{24} cage.

Effect of solvent on the vibrational spectra: To investigate the effect of including solvent in the computational modelling, the IR spectrum of the $[Mo_2O_7]^{2-}$ ion was calculated by using solvents with dielectric constants, ε, between 0 and 100. This ion shows two strong absorptions in its IR spectrum,[30,31,32] at 783–795 and 880–885 cm^{-1} and corresponding to stretching of the bridging and terminal Mo–O bonds respectively. There is a further weak feature around 300 cm^{-1}, corresponding to a bending motion of, primarily, the terminal metal–oxygen bonds. At the LDA/TZP level, the Mo–O_t and Mo–O_{2c} bond length[21] are 1.77 and 1.93 Å respectively and do not change appreciably when the solvent is included.

Figure 4 shows the calculated IR trace for $[Mo_2O_7]^{2-}$ using model solvents with increasing dielectric constant. Computationally the solvent has two effects. Firstly, there is a shift of all three bands to lower frequency as the dielectric constant is increased. This is very pronounced between $\varepsilon = 0$ and $\varepsilon = 20$. As the dielectric constant is increased further, there is a consistent but much smaller reduction in the frequencies. Secondly, the intensity of the bands increases as the dielectric constant is increased. Again, this change is largest between between $\varepsilon = 0$ and $\varepsilon = 20$. It may be noted that the pseudo-gas phase calculation yields vibrational frequencies in best agreement with experiment.

The Mulliken charges on the atoms are affected by the introduction of solvent: for $\varepsilon = 0$, $q_{Mo} = 1.84$ and for $\varepsilon = 20$, $q_{Mo} = 1.98$. Increasing the dielectric constant of the solvent leads to only a small increase in this charge. Thus, the solvent field increases the polarity of metal–oxygen bonds and this is reflected in a decrease in the covalent bond order: for $\varepsilon = 0$, Mo–$O_{t=}$1.56, Mo–$O_{2c} = 0.69$ and for $\varepsilon = 20$, Mo–O_t = 1.50 and Mo–$O_{2c} = 0.69$. The decrease in the bond order and the associated increase in the dipole moments of each bond presumably lead to the reduced vibrational frequencies and the increased IR intensity found in the modelling.

To investigate the effect of solvent on the computational model for the Anderson POMs, additional vibrational analyses were carried out on $[TeMo_6O_{24}]^{6-}$ and $[IMo_6O_{24}]^{5-}$ at the LDA/TZP level in water ($\varepsilon = 78.4$) and at the BP86/TZP level in vacuo and in water. For an additional comparison, in vacuo calculations were also performed at the B3LYP/LANL2DZ(P) level. The calculated IR traces for $[TeMo_6O_{24}]^{6-}$ and $[IMo_6O_{24}]^{5-}$ obtained by using these methods are shown in Figure 5 and Figure 6, respectively.

A comparison of pseudo-gas phase calculations suggests that, for these ions, the LDA and BP86 approaches yield quite similar frequencies whilst the B3LYP method gives significantly lower frequencies. For the telluromolybdate, the BP86 frequencies are actually in slightly better agreement with the available experimental results than those obtained at the LDA level. For the iodomolybdate, this situation is reversed. As noted above, both methods tend to underestimate the frequencies, particularly for the most intense bands due to the Mo–O and X–O stretching modes. As previously observed for Anderson[6] and Keggin[7,8] anions, this result is even more pronounced at the B3LYP level. It should be noted, however, that the inclusion of additional polarization functions in the LANL2DZ basis set in

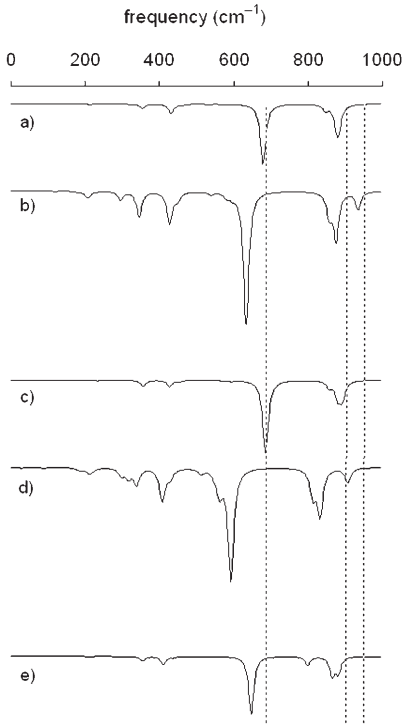

Figure 5. Calculated IR trace for $[TeMo_6O_{24}]^{6-}$ at the a) LDA/TZP, b) LDA/TZP/Sol, c) BP86/TZP, d) BP86/TZP/Sol and e) B3LYP/LANL2DZ(P) levels. The dotted lines indicate the positions of the most intense absorptions in the experimental spectrum.

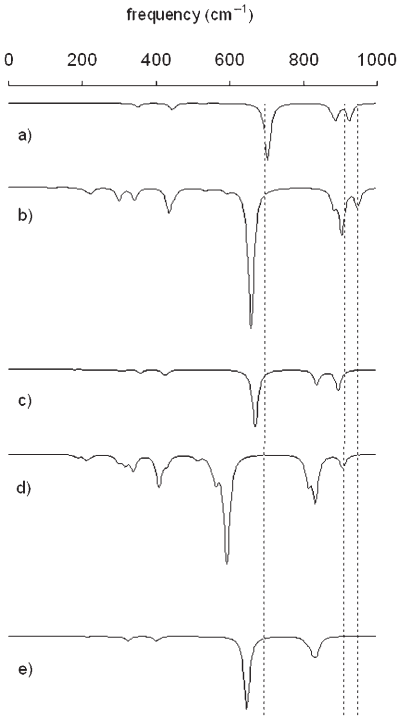

Figure 6. Calculated IR trace for $[IMo_6O_{24}]^{5-}$ at the a) LDA/TZP, b) LDA/TZP/Sol, c) BP86/TZP, d) BP86/TZP/Sol and e) B3LYP/LANL2DZ(P) levels. The dotted lines indicate the positions of the most intense absorptions in the experimental spectrum.

the present study led to significantly improved results. In our previous work on anions with lower charge, such functions were not included. They are recommended for vibrational studies using the B3LYP functional on POMs.

As found for the simple $[Mo_2O_7]^{2-}$ ion, inclusion of solvent in the model leads to an increase in the absorption intensity. For both the telluro and iodo systems, this is most notable at the LDA level and for the intense e_u (ν_{46}) band. Table 4 lists atomic charges and bond orders for the $[TeMo_6O_{24}]^{6-}$ and $[IMo_6O_{24}]^{5-}$ ions at the LDA/TZP level, calculated in the gas phase and in water at the respective optimized geometries. As noted above, for the $[Mo_2O_7]^{2-}$ ion, inclusion of solvent leads to an increase in the charge of the metal and a decrease in the bond order. For $[IMo_6O_{24}]^{5-}$, there is also a small increase in the ionicity with small increases in the molybdenum, iodine and bridging oxygen charges. However, this is not accompanied by significant decreases in the covalent bond orders. For $[TeMo_6O_{24}]^{5-}$, the atomic charges of the Mo, Te and terminal O sites are actually somewhat smaller in the solvated environment. Accompanying this are increases in the covalent bond order, particularly for the Mo–O_t.

As shown in Figure 5 and Figure 6, the effect of the solvent on the calculated frequencies is also less straightforward than the universal shift to lower frequencies observed for dimolybdate. For $[TeMo_6O_{24}]^{5-}$ and $[IMo_6O_{24}]^{6-}$, the intense e_u (ν_{46}) band shifts to significantly lower frequency when solvent is included at both the LDA and BP86 levels. This mode corresponds to the asymmetric stretching of the Mo–O_{2c} bonds. In the absence of solvent, the e_u (ν_{44}) and a_{2u} (ν_{35}) bands at higher frequency, corresponding to Mo–O_t stretching modes, in the spectrum of $[TeMo_6O_{24}]^{5-}$ overlap. When solvent is included, the a_{2u} (ν_{35}) band is not appreciably shifted but the e_u (ν_{44}) mode shifts by ca. 50 cm^{-1} to *higher* frequency. Although these bands do not overlap in the iodo system, the effect of the solvent on their frequen-

Table 4. Bond orders and atomic charges for $[TeMo_6O_{24}]^{6-}$ and $[IMo_6O_{24}]^{5-}$ calculated at the LDA/TZP and LDA/TZP/Sol levels.

	$[TeMo_6O_{24}]^{6-}$					$[IMo_6O_{24}]^{5-}$				
charges	Mo	Te	O_t	O_{2c}	O_{3c}	Mo	I	O_t	O_{2c}	O_{3c}
LDA/TZP	2.14	2.74	−0.82	−0.93	−1.03	2.01	3.02	−0.75	−0.88	−0.96
LDA/TZP/Sol	2.04	2.70	−0.78	−0.93	−1.02	2.07	3.08	−0.75	−0.92	−0.99
bond orders:	Mo–O_t	Mo–O_{2c}	Mo–O_{3c}	Te–O		Mo–O_t	Mo–O_{2c}	Mo–O_{3c}	I–O	
LDA/TZP	1.51	0.69	0.30	0.66		1.59	0.72	0.28	0.70	
LDA/TZP/Sol	1.56	0.70	0.32	0.68		1.58	0.70	0.28	0.70	

cies is similar. Experimentally, the high frequency region consists of two bands and the inclusion of solvent appears to improve both their resolution and frequencies in the modelling. Solvent appears to have a slightly greater effect at the LDA level, presumably as it helps to compensate the overbinding that occurs with this functional.

Figure 7 shows the calculated IR spectrum for the Lindqvist isopolyanion $[Mo_6O_{19}]^{2-}$ in the absence and in the presence of solvent. As observed for $[Mo_2O_7]^{2-}$, inclusion of solvent leads to a decrease in the calculated frequencies of all

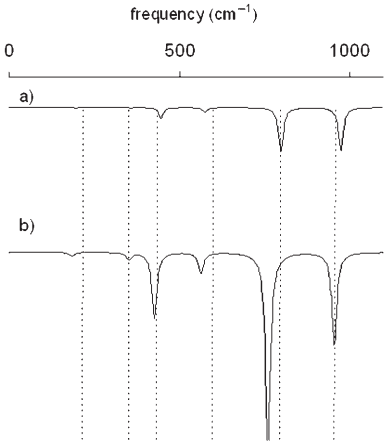

Figure 7. Calculated IR trace for $[Mo_6O_{19}]^{2-}$ at the LDA/TZP level with a) no solvent and b) inclusion of water solvent. The dotted lines indicate the positions of the most intense absorptions in the experimental spectrum.[6]

bands. No appreciable change in the Mo–O bond length is observed at the LDA/TZP level when solvent is included. For the $[Mo_6O_{19}]^{2-}$ and $[Mo_2O_7]^{2-}$ ions, solvent therefore appears to have little effect on the calculated bond lengths and the reduction in the vibrational frequencies can be associated with the increased polarity and decreased covalency of the bonding. It is probable that the higher negative charged associated with the Anderson anions leads to a contraction of the clusters, as shown in Table 1. These structural changes together with changes in the character of the bonding lead to more significant shifts in the calculated frequencies. The direction of the shifts depend on the bond type with the bands due to stretching of the Mo–O_{2c} bonds shifted to lower frequencies and the bands due to stretching of the Mo–O_t bonds unshifted or even shifted to higher frequency.

Conclusion

High level density functional methods have been used to calculate the structure and vibrational frequencies of the Anderson $[TeMo_6O_{24}]^{5-}$ and $[IMo_6O_{24}]^{6-}$ heteropolyanions. These ions are classified as type-II POMs as each molybdenum atom is bonded to two *cis*-related Mo–O_t groups. These calculations represents the first high-level computational study of the vibrational spectra of type-II ions and in general, the agreement between the calculated unscaled vibrational frequencies and those determined experimentally is very good allowing the spectra to be assigned. Raman intensities of a POM have also been calculated for the first time.

Table 5 lists characteristic group frequencies for type I and II POMs based on the present study and our previous computational studies of Lindqvist[6] and Keggin anions.[7,8]

Table 5. Characteristic group frequencies for type I and type II polyoxometalates.

	α and β-$[XMo_{12}O_{40}]^{z-}$		$[Mo_6O_{19}]^{2-}$		$[XMo_6O_{24}]^{z-}$	
ν (X–O)	IR	940–1060			R	680–685
	IR	800–960			IR	540–635
ν (Mo–O_t)	R	960–999	R	980–999	R	900–960
	IR	920–980	IR	957–970	IR	900–960
	R	920–980	R	951–968		
ν_s (Mo-O_{2c1}-Mo)	R	600–630			R	690–720
	IR	700–810	IR	796–810	IR	690–72
ν_{as} (Mo-O_{2c2}-Mo)	IR	770–900				
ν_s (Mo–O_a)	R	245–247	R	278–290		

The Mo–O_t bonds in the type I systems tend to vibrate at slightly higher frequencies than for the type II anions, as might be anticipated on the basis of the formal bond orders of 2.5 and 2 respectively.[21] The bands due to stretching of the Mo–O_{2c} bonds also occur at somewhat lower frequency in the type II anions. The heteroatom–oxygen bonds vibrations at significantly lower frequency in the Anderson anions than in the Keggin anions and this may be simply related to the higher coordination number of the heteroatom in the former.

For the first time, the effect of solvent on the computational model has been investigated. For $[Mo_2O_7]^{2-}$ and $[Mo_6O_{19}]^{2-}$, inclusion of solvent has little affect on the bond lengths but leads to lower vibrational frequencies. For the Anderson anions, the situation is found to be more complicated with inclusion of solvent leading to contraction of the anion, a decrease in the vibrational frequencies due to stretching of the Mo–O_{2c} bonds but an increase in the frequencies due to stretching of the Mo–O_t bonds. For these highly charged anions, inclusion of some of the environmental effects experienced in the solution or solid phase using a simple solvent model appears to improve the accuracy of the modelling.

Acknowledgements

The author would like to the University of Hull for financial support and the UK Computational Chemistry Working Party for access to computational facilities in the Rutherford Appleton Laboratory.

[1] M. T. Pope, *Heteropoly and Isopoly Oxometalates*, Springer, Heidelberg, **1983**.
[2] M. T. Pope, A. Müller, *Angew. Chem.* **1991**, *103*, 56; *Angew. Chem. Int. Ed. Engl.* **1991**, *30*, 34.
[3] L. C. W. Baker, D. C. Glick, *Chem. Rev.* **1998**, *98*, 3.
[4] M. T. Pope, A. Müller, *Polyoxometalates: from Platonic Solids to Anti-Retroviral Activity*, Kluwer: Dordrecht, **1994**.
[5] R. I. Buckley, R. J. H. Clark, *Coord. Chem. Rev.* **1985**, 65, 167.
[6] A. J. Bridgeman, G. Cavigliasso, *Chem. Phys.* **2002**, *279*, 143.
[7] A. J. Bridgeman, *Chem. Phys.* **2003**, *287*, 55.
[8] A. J. Bridgeman, *Chem. Eur. J.* **2004**, *10*, 2935.
[9] X. Lopez, C. Nieto-Draghi, C. Bo, J. B. Avalos, J. M. Poblet, *J. Phys. Chem. A* **2005**, *109*, 1216.
[10] X. Lopez, J. A. Fernandez, S. Romo, J. F. Paul, L. Kazansky, J. M. Poblet, *J. Comput. Chem.* **2004**, *25*, 1542.
[11] G. te Velde, F. M. Bickelhaupt, E. J. Baerends E. J. , G. Fonseca Guerra, J. G. Snijders, T. Ziegler, *J. Comput. Chem.* **2001**, *22*, 931; C. Fonseca Guerra, J. G. Snijders, G. te Velde, E. J. Baerends, *Theor. Chem. Acc.* **1998**, 99, 391.
[12] ADF2002.02, SCM, Theoretical Chemistry, Vrije Universiteit, Amsterdam, The Netherlands, http://www.scm.com
[13] S. H. Vosko, L. Wilk, M. Nusair, *Can. J. Phys.* **1980**, *58*, 1200.
[14] A. D. Becke, *Phys. Rev. A* **1988**, 38, 3098; J. P. Perdew, *Phys. Rev. B* **1986**, 33, 8822.
[15] P. J. Stephens, F. J. Devlin, C. F. Chabalowski, M. J. Frisch, *J. Phys. Chem.* **1994**, *98*, 11 623.
[16] Gaussian 98, Revision A.3, M. J. Frisch, G. W. Trucks, H. B. Schlegel, G. E. Scuseria, M. A. Robb, J. R. Cheeseman, V. G. Zakrzewski, J. A. Montgomery Jr, R. E. Stratmann, J. C. Burant, S. Dapprich, J. M. Millam, A. D. Daniels, K. N. Kudin, M. C. Strain, O. Farkas, J. Tomasi, V. Barone, M. Cossi, R. Cammi, B. Mennucci, C. Pomelli, C. Adamo, S. Clifford, J. Ochterski, G. A. Petersson, P. Y. Ayala, Q. Cui Q., K. Morokuma, D. K. Malick, A. D. Rabuck, K. Raghavachari, J. B. Foresman, J. Cioslowski, J. V. Ortiz, B. B. Stefanov, G. Liu, A. Liashenko, P. Piskorz, I. Komaromi, R. Gomperts, R. L. Martin. D. J. Fox, T. Keith, M. A. Al-Laham, C. Y. Peng, A. Nanayakkara, C. Gonzalez, M. Challacombe. P. M. W. Gill, B. Johnson B, W. Chen W, M. W. Wong, J. L. Andres J. L., C. Gonzalez, M. Head-Gordon, E. S. Replogle, J. A. Pople, Gaussian, Inc., Pittsburgh PA, **1998**.
[17] A. Klamt, G. Schûûrmann, *J. Chem. Soc. Perkin Trans. 1* **1993**, 2, 799; J. Andzelm, C. Kõlel, A. Klamt, *J. Chem. Phys.* **1995**, *103*, 9312; A. Klamt, *J. Chem. Phys.* **1995**, 99, 2224. Model implemented in ADF by C. C. Pye, T. Ziegler, *Theor. Chem. Acc.* **1999**, *101*, 396.
[18] spectralPlot. A Java applet to plot spectral traces from the output of the electronic structure packages Gaussian98 and ADF, written by A. J. Bridgeman, University of Hull, 2002, http://www.hull.ac.uk/chemistry/plotSpectralData.php
[19] I. Mayer, *Chem. Phys. Lett.* **1983**, *97*, 270; I. Mayer, *Int. J. Quantum Chem.* **1984**, *26*, 151.
[20] A. J. Bridgeman, C. J. Empson, *MAYER*, The University of Hull, Hull, U. K., **2003**. Freely available on the worldwide web from http://www.hull.ac.uk/php/chsajb/mayer.
[21] A. J. Bridgeman, C. E. Cavigliasso, *J. Phys. Chem. A* **2003**, *107*, 6613.
[22] C. Robl, M. Frost, *Z. Naturforsch. B* **1993**, 48, 404; P. A. Lorenzo-Luis, P. Gili, A. Sanchez, E. Rodriguez-Castellón, J. Jiménez-Juménez, C. Ruiz-Pérez, X. Solans, *Trans. Metal. Chem.* **1999**, *24*, 686.
[23] H. Kondo, A. Kobayashi, Y. Sasaki, *Acta. Crystallogr. Sect. B* **1980**, 36, 661.
[24] J. M. Poblet, X. Lopez, C. Bo, *Chem. Soc. Rev.* **2003**, *32*, 297.
[25] A. J. Bridgeman, G. Cavigliasso, *J. Phys. Chem. A* **2001**, *105*, 7111.
[26] A. J. Bridgeman, G. Cavigliasso, *Faraday Discuss.* **2003**, 124, 239.
[27] R. Grabowski, A. Gumuka, J. Sloczynski, *J. Phys. Chem. Solids* **1980**, *41*, 1027.
[28] A. C. Dengel, W. P. Griffith, S. I. Mostafa, A. J. P. White, *Spectrochim. Acta Part A* **1993**, 49, 1583.
[29] Animations of the IR and Raman active modes of $[TeMo_6O_{24}]^{6-}$: http://www.hull.ac.uk/chemistry/pom.
[30] V. W. Day, M. F. Fredrich, W. G. Klemperer, W. Shum, *J. Am. Chem. Soc.* **1977**, *99*, 6146.
[31] P. Braunstein, C. D. de Bellofon, M. Lanfranchi, A. Tiripicchio, *Organometallics* **1984**, *3*, 1772.
[32] R. G. Battacharyya, S. Biswas, *Inorg. Chim. Acta* **1991**, 181, 213.

Received: July 12, 2005
Published online: December 16, 2005

